Tunable Properties of Self-Assembled Polyurethane Using Two-Dimensional Nanoparticles: Potential Nano-biohybrid

ARTICLE *in* MACROMOLECULES · NOVEMBER 2010

Impact Factor: 5.8 · DOI: 10.1021/ma101909j

5 AUTHORS, INCLUDING:

Biswa P. Das Purkayastha
Assam University
9 PUBLICATIONS **96** CITATIONS
SEE PROFILE

Vinod K Aswal
Bhabha Atomic Research Centre
392 PUBLICATIONS **4,906** CITATIONS
SEE PROFILE

Pralay Maiti
Indian Institute of Technology (Banaras Hin…
102 PUBLICATIONS **3,640** CITATIONS
SEE PROFILE

DOI: 10.1021/ma101909j

Macromolecules
ARTICLE

Tunable Properties of Self-Assembled Polyurethane Using Two-Dimensional Nanoparticles: Potential Nano-biohybrid

Abhinay Mishra,[†] Biswa Pratim Das Purkayastha,[‡] Jagat K. Roy,[‡] Vinod K. Aswal,[§] and Pralay Maiti*,[†]

[†]*School of Materials Science and Technology, Institute of Technology, Banaras Hindu University, Varanasi 221 005, India,* [‡]*Department of Zoology, Banaras Hindu University, Varanasi 221 005, India, and* [§]*Solid State Physics Division, Bhabha Atomic Research Centre, Trombay, Mumbai 400 085, India*

Received August 20, 2010; Revised Manuscript Received October 7, 2010

ABSTRACT: Nanostructure, key to property alteration, has been widely diverse by using two-dimensional nanoparticle in different stages of polymerization. Molecular level self-assembly starting from nanoscale 2-D molecular sheet to optically observable microscale crystallite has been unraveled stepwise for thermoplastic elastomer for the first time. The nature of self-assembly can be tuned by judicious choice of polymerization procedure in the presence of organically modified nanoclay. The effect of modulated nanostructure and self-assembly has been explored for the unusual property enhancement including electronic, thermal, mechanical, barrier, and biological (genotoxicity). Both the stiffness and toughness increase in nano-biohybrid without any trade-off. The unique splintering phenomenon and its variation under a dynamic frequency have been investigated by changing the synthesizing route of nanohybrids using a fixed concentration of nanoparticle. For understanding the controlled cellular responses to the implant new hybrid materials, cell adhesion and detailed genotoxicity reveal total biological recognition of the developed nano-biohybrids.

Introduction

The early path breaking work of Otto Bayer on versatile polyurethanes (PU) is diversified to meet the demand of modern technologies like coating, adhesive, foams, composites, and advanced biomaterials.[1−5] The properties of PU can be tailored either by varying the chemical nature and composition of polyol, diisocyanate, and chain extender or by dispersing fillers in a polymer matrix.[6−11] A wide variety of fillers are being used to improve the properties of polymer which in turn depend on the shape, size, aspect ratio, and surface modification of the fillers, e.g., whiskers and fibers were found effective in matrix reinforcement with lowered toughness and fluoromica for enhanced ductility with lesser stiffness.[12] However, a trade-off has been observed in most cases limiting the use of hybrid materials as potential biomaterials. Improving the overall performance requires enhancing the stiffness and toughness together with their tunability depending on particular application especially in biomedical use.

Polymeric self-assemblies have advantages over conventional micelles from surfactants such as better stability, superior mechanical properties, and obtaining metastable structure.[13,14] Importantly, chemical, physical, and biological properties can be tailored using polymeric self-assemblies by varying chemical structure or size of the constituents. Self-assemblies are more familiar for block copolymer[15−18] and dendritic polymer[19−23] because of thermodynamic incompatibility of the components ensuing stimuli responsiveness such as control release of encapsulated substances while exposed to pH, solvent, and thermal sensitive systems. However, many potential applications require supramolecular aggregates, whose properties might be tuned by controlling the dimension of assemblies either chemically or in the presence of inorganic fillers. Poly(3-hexylthiophene) is a typical homopolymer where close π-stacking of the adjacent polymer chains leads to strong electronic coupling, thereby forming "2-D" sheets in which the side chains separate layers of interacting conjugated moieties.[24,25] It would be of immense interest if sheet-type organization can be generated in conventional thermoplastics leading to patterned structure. A part of the present work is devoted to the designing of self-assembled patterns in pure thermoplastic polyurethane and tuning of self-aggregation by using 2-D inorganic nanoparticles.

Biological recognition of synthetic biomaterials depends on the cell adhesion to materials which is initiated by cell−surface receptor, interacting with cell adhesion protein bound to the materials surface.[26] These materials have been patterned in different dimensions to generate model multicellular tissue architectures, and this approach may be useful to generate complex organization of multiple cell types. DNA damage or genotoxic stress is believed to signal the activation of a number of kinases, which in turn activates p53 by phosphorylating it at different regions.[27] Among the different kinases getting activated upon DNA damage, HIPK2 (Homeodomain Interacting Protein Kinase 2), a member of the serine/threonine kinase, is stabilized. A fraction of this stabilized nuclear HIPK2 is recruited to the PML (promyelocytic leukemia) nuclear bodies.[28] This HIPK2 then phosphorylates p53 at Ser46, which results in the activation of the apoptotic response.[29] This can be further substantiated by the fact that p53-dependent apoptosis is decreased considerably in HIPK2 knockdown and increased in chemotherapeutically treated cells.[30] The proapoptotic function is dependent on its subcellular localization. The apoptotic index has been found to be considerably high in the case of the nuclear localization of HIPK2. Cytoplasmic localization of the protein has an antagonistic effect on the index.[31] This means that the nuclear localization of HIPK2 is an indicator of its active state, and its localization to the cytoplasm renders it inactive. Considering the importance of the subcellular localization of HIPK2 in providing insight into the internal environment of the cells, we used this as a

*To whom correspondence should be addressed. E-mail: pmaiti.mst@itbhu.ac.in.

 Published on Web 11/16/2010

tool to check whether the incorporation of nanoparticles in polyurethane is biologically compatible or not, when used as a surface for growth or adherence.

Experimental Section

Materials. Poly(tetramethylene glycol) (PTMG) (terathane, Sigma-Aldrich; number-average molecular weight (M_n = 2900 g/mol), 1,6-hexamethylene diisocyanate (HDI), and 1,4-butanediol (BD) (Merck, Germany) were used as received. Organically modified nanoclay was methyl tallow bis-hydroxyethyl quaternary ammonium ion-exchanged montmorillonite (Southern Clay, CEC 110 mequiv/100 g) (Cloisite 30B). The catalyst dibutyltin dilaurate and solvent dimethylformamide (DMF) were purchased from Himedia and Loba Chemie, respectively.

Synthesis of Polyurethanes and Its Nanocomposites. The polyurethanes (PU) were synthesized in two steps: prepolymer preparation using PTMG and HDI followed by addition of chain extender (BD: required amount in 5 mL of DMF solvent) and catalyst (DBTDL: 0.1 ml of 1 wt % toluene solution) to complete the polymerization reaction with rapid stirring at 70 °C for 24 h. The molar ratio of PTMG:HDI:BD was kept at 1:3.2:2.2, respectively. The polymer was extracted by pouring the solution in deionized water (nonsolvent for PU) and dried in vacuum at reduced pressure at 60 °C for 48 h. The hard segment content was kept constant (20%) by using a predetermined amount of polyol, diisocyanate, and chain extender. Nanocomposites were synthesized by mixing 4 wt % 30B nanoclay at various stages during polymerization process following the schemes below with the designation of nanocomposites. The molecular weights of pure PU and its nanocomposites are ~35 000 (PDI ~ 1.8) as measured using gel permeation chromatography using DMF as eluent at 70 °C with 1 mL/min flow rate. The following reaction schemes have been used to prepare nanohybrids with their designations:

$$\mathrm{PTMG + nanoclay \longrightarrow mix \xrightarrow{HDI} mix \xrightarrow[DBTDL]{BD} PTMG-NC} \quad (1)$$

$$\mathrm{PTMG + HDI \longrightarrow mix \xrightarrow{nanoclay} mix \xrightarrow[DBTDL]{BD} PP-NC} \quad (2)$$

$$\mathrm{PTMG + HDI \longrightarrow mix \xrightarrow[DBTDL]{BD} mix \xrightarrow{nanoclay} PI-NC} \quad (3)$$

$$\mathrm{PU \xrightarrow[solvent]{nanoclay} SI-NC} \quad (4)$$

Nanostructure and Self-Assembly. X-ray diffraction was performed using a Bruker AXS D8 Advance wide-angle X-ray diffractometer with a graphite monochromator using Cu Kα source with a wavelength of 0.154 nm. The generator was operated at 40 kV and 20 mA. The thin sheets of the samples, prepared by using the compression-molding technique, were placed on a glass sample holder at room temperature and were scanned at diffraction angle 2θ from 1° to 40° at the scanning rate of 1° min^{-1}.

Small-angle neutron scattering (SANS) experiments were performed on the spectrometer at the Dhruva reactor at Bhabha Atomic Research Centre, Mumbai, India. The data were collected in the scattering vector (q) range of 0.17 $nm^{-1} \leq q \leq$ 3.5 nm^{-1}. The scattering from the samples were corrected for background contribution. The lower q range was fitted separately with Ornstein−Zernike and other models. The characteristics length (Λ_c) was calculated using the equation $\Lambda_c = 2\pi/q_m$, where q_m is the scattering vector q corresponding to the peak position of the shoulder in the scattering pattern. The temperature was kept constant at 30 °C during every measurement.

The degree of crystallinity, melting, crystallization temperatures, and heats of fusion of the pure PU and its nanocomposites were determined via differential scanning calorimetry (DSC) using a Mettler 832 over a temperature range of −100 to 200 °C at a scan rate of 10 °C min^{-1}. The samples were heated at the scan rate of 10 °C min^{-1}. The peak temperature and enthalpy of fusion for first run were measured from the endotherms using a computer attached with the instrument. After the first melting, the samples were quenched at 100 °C min^{-1} to find the glass transition temperature. The peak temperature and enthalpy of fusion for the second run were also measured. The DSC was calibrated with indium before use.

The UV−vis measurements have been carried out by using a Shimadzu (UV-1700), Pharma Speck, UV−vis spectrophotometer operating in the spectral range of 200−1100 nm using a thin solid film. FTIR was performed in absorbance measurement mode at room temperature from 400 to 4000 cm^{-1} using a Nicolet 670 with a resolution of 4 cm^{-1}.

The morphology of pure PU and its nanocomposites was investigated by using scanning electron microscope (SEM), atomic force microscope (AFM), and polarizing optical microscope (POM). The nanoclay dispersion in the matrix was checked by using TEM (Technai G^2) operated at an accelerating voltage of 100 kV. A thin layer, around 70 nm thick, from the nanocomposite sample was sectioned at −80.0 °C using a Leica ultramicrotome equipped with a sharp glass knife. The surface morphology of polyurethane nanocomposite flakes was examined with a Hitachi H-7100 scanning electron microscope operated at an accelerating voltage of 10 kV. All the samples were gold-coated by means of a sputtering apparatus under vacuum before observation. Atomic force microscopy was performed using a NT-MDT multimode AFM, Russia, controlled by a Solver scanning probe microscope controller. Tapping mode was used with the tip mounted on 100 μm long, single beam cantilever with resonant frequency in the range 240−255 kHz and the corresponding spring constant of 11.5 N/m. Bulk morphology of thin film (~30 μm) in optical range was examined using a polarizing optical microscope (POM) (Leitz) after quenching the samples at room temperature on a Mettler hot stage.

Mechanical Properties and Network Splintering. For tensile testing, standardized specimens were prepared via microinjection using a microinjector (model FD-1, Fly Tech Engineering). The samples were microinjected at a barrel temperature of T_m + 20 °C and mold temperature of 25 °C with a pressure of 100 bar. The melting point of pure PU is 165 °C, and the T_m of other nanocomposites has been presented in Figure 3b. Tensile tests were performed with the injection-molded samples using an Instron 3369 tensile tester at a strain rate of 5 mm/min at room temperature with specimen dimensions of 25 mm gauge length, 4.05 mm breadth, and 2.12 mm thickness. Several samples were tested to obtain good error estimates. The frequency dependence of oscillatory shear moduli in the liquid state was measured, using dynamic frequency sweep tests, on a Rheologica (model: Nova) using parallel plate geometry (25 mm) at the constant temperature of 150 °C, keeping the strain amplitude of 0.05 to maintain linear response of the sample. The measured angular frequency ω for oscillatory shear experiment was kept in the range from 0.5 to 300 rad/s. The storage moduli and complex viscosities were measured as a function of angular frequency for pure PU and its nanocomposites. Scratch hardness was measured by scratching a polymer/hybrid-coated (~40 μm) steel panel with a needle under varying weight to get an electrical signal out of metallic contact.

Cell Adhesion and Genotoxicity. HeLa and SiHa cells were cultured on glass substrate for 24 h in DMEM supplemented with 10% heat-inactivated FCS (GIBKO) and antibiotics in a humidified 5% CO_2 incubator at 37 °C. The cells were washed with 1X PBS and then treated with cisplatin (Fresenius Kabi Oncology Ltd., India) at the concentration of 3, 4, 5, and 6 μg mL^{-1} in a fresh media for 24 h. The cells were then washed two times with 1X PBS, and fixation was done in 4% PFA for 10 min. The fixed cells in the coverslip were washed and

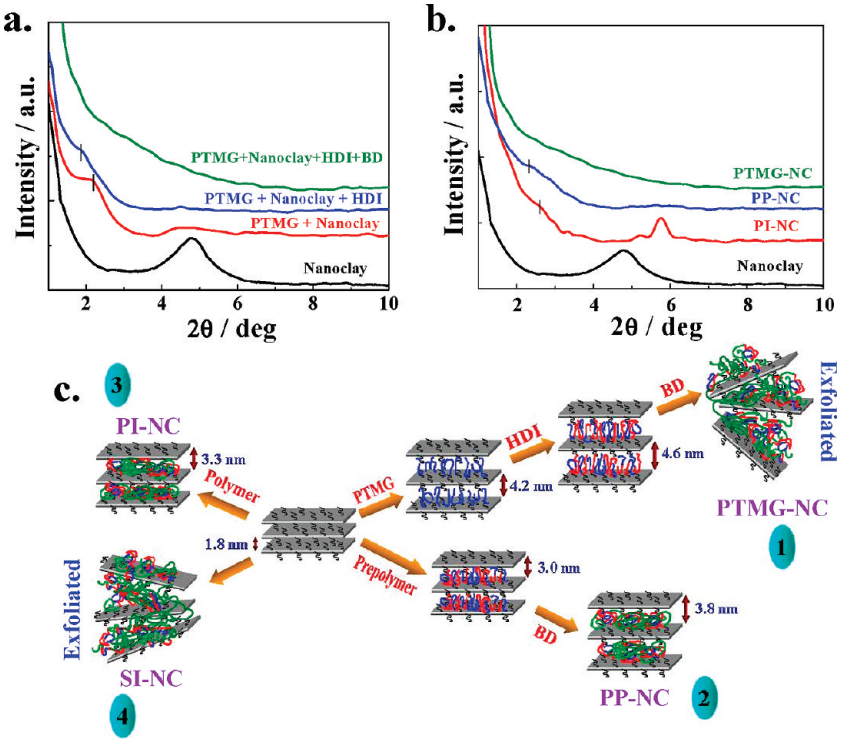

Figure 1. (a) Wide-angle X-ray diffraction of organically modified Closite-30B nanoclay and intermediates formed at different stages during the synthesis of PTMG-NC nanocomposites. (b) X-ray diffraction patterns of organically modified Closite-30B nanoclay and nanocomposites. (c) Schematic representation for alteration of intergallery spacing (through XRD) of nanoclay and polyurethane nanocomposites, synthesized via addition of nanoclay at the different stages of the polymerization process. Processes 1, 2, and 3 represent the synthesis of PTMG-NC, PP-NC, and PI-NC, respectively, while process 4 shows the solution-casting synthesis of nanocomposites using DMF solvent. Scheme defines the changes of intergallery spacing obtained from XRD for the different processes; PTMG-NC nanocomposite is exfoliated while PP-NC and PI-NC are intercalated.

permeablized with 0.1% PBST (1X PBS + 0.1% Triton X-100) for 10 min each and subsequently blocked with blocking solution (1X PBS, 0.1% sodium deoxycholate, 0.1% Triton-X, 0.1% BSA, 10% fetal calf serum, 0.02% Thiomersal) at room temperature for 2 h. Primary antibody (Goat anti-HIPK2, Santa Cruz Biotech. Inc. at the dilution of 1:200) incubation was for overnight at 4 °C and was washed twice for 10 min with 0.1% PBST. Precleared secondary antibody (Donkey antigoat Cy3, Molecular Probes at the dilution of 1:200) was incubated for 2 h at room temperature. The cells were again washed for 10 min twice with 0.1% PBST followed by counterstaining with DAPI (4′,6-diamidino-2-phenylidone dihydrochloride, Sigma) for 15 min. A single wash with 0.1% PBST was done, and finally slides were mounted with DABCO (antifading agent). For estimation of the percentage of cells showing nuclear or cytoplasmic localization of the protein, a Nikon E800 microscope was used, and optical image was collected from a confocal microscope (Zeiss: LSM 510Meta). The images were modified in Adobe Photoshop. Thin film of polymer and its nanocomposites were coated onto glass substrate to check whether the polymers are toxic for the cells. The polymer and composites coated glass were then sterilized by using UV irradiation for 2 h, and then cells were seeded onto them along with control (5 μg mL^{-1} of cisplatin). The cells were then processed as above.

Results and Discussion

Wide Variation in Nanostructure. The effect of step-by-step addition of the constituents of polyurethane on the basal spacing of layered silicate has been shown in Figure 1a. The (001) peak of nanoclay (d_{001} = 1.8 nm; $2\theta \sim 4.8°$) has been shifted to lower angle, and the corresponding *d*-spacing of organically modified nanoclay increases to 4.2 nm ($2\theta \sim 2.19°$) on addition of poly(tetramethylene glycol) (PTMG; polyol) due to intercalation. The subsequent addition of hexamethylene diisocyanate (HDI) increases the spacing to 4.6 nm ($2\theta \sim 1.86°$) as prepolymer formation occurs in the gallery, and interestingly, after adding the chain extender, butanediol (BD), the (001) peak disappears, indicating exfoliated structure because of further chain expansion within the gallery leading to push apart the individual nanoclay layer to a great extent. In this case, polymerization was occurring inside the nanoclay galleries. On the other hand, lesser intercalation occurs if a prepolymer (product of the reaction of HDI and PTMG) and polymer (reaction product of prepolymer and chain extender) was formed separately, and subsequently nanoclay was added to them (Figure 1b). The schematic of polymerization, addition of nanoclay, and subsequent basal spacing have been presented in Figure 1c describing the outcome of *d*-spacing arising from all four possible ways of preparing polyurethane nanocomposites, namely PTMG-NC (PTMG intercalation; nanoclay added to PTMG), PP-NC (prepolymer intercalation; nanoclay added to prepolymer), PI-NC (polymer intercalation; nanoclay added to polymer), and SI-NC (solution intercalation: adding nanoclay into dilute solution of polymer). So, one can generate a wide ranges of nanostructure by adding nanoclay at different stages of polymerization. The crystallite dimension, as calculated using the Scherrer equation ($D_{hkl} = k\lambda/(\beta \cos \theta)$), are 25 and 17 nm for PI-NC and PP-NC, respectively, and believed to negligibly small for PTMG-NC as suggested from the absence of any peak in the XRD pattern. The distribution of nanoclay in matrix is confirmed through TEM images and PTMG-NC exhibit exfoliated pattern (correlation length, χ = 55 ± 5 nm) while PI-NC shows highly intercalated nature (χ = 300 ± 20 nm) and PP-NC displays the intermediate intercalation performance (χ = 80 ± 10 nm) (Figure 2a). Hence, TEM images support the

XRD patterns of the corresponding nanocomposites. Moreover, the average lateral dimension of nanoclay also changes from 200, 300, and 600 nm for PTMG-NC, PP-NC, and PI-NC, respectively, indicating flocculating nature of nanoclay with increasing stack size of tactoids. The lateral dimension of pristine organically modified nanoclay (~200 nm) is the same for exfoliated PTMG-NC while flocculation increases for intercalated nanocomposites when the interaction between polymer chains and nanoclay is moderate. The intercalation is limited for bigger chains cf. prepolymer and polymer while they are added to nanoclay directly, but when both the chain expansion process occurs in the gallery, the bigger chains within are capable to exfoliate the nanoclay layers bonded through weak van der Waals forces during the polymerization process. The greater intercalation has been observed in aliphatic polyurethane, against limited intercalation (up to ~5 nm) for bulkier aromatic PU reported in the literature, due to enhanced interaction in case of aliphatic PU.[32,33] The enhanced order of interaction (PI-NC < PP-NC < PTMG-NC) has also been confirmed from the gradual red shifting of the UV−vis absorption peak of pure nanoclay at 244 nm to 256, 275, and 285 nm for PI-NC, PP-NC, and PTMG-NC, respectively (Figure 2b). The appearance of absorption peak is due to the $\pi \rightarrow \pi^*$ transition of the double bond present in organic modifier of the nanoclay. However, the properties of nanocomposites depend on the nanostructure, and hence, one can tune the properties by suitably synthesizing the nanocomposites or by adding the nanoparticles in various stages of polymerization.

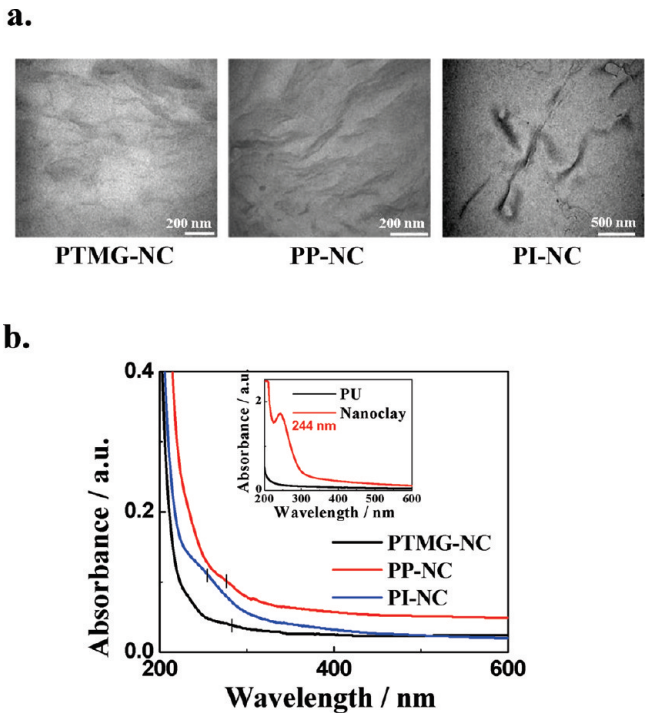

Figure 2. (a) Bright field transmission electron micrographs of indicated PU nanocomposites. (b) UV−vis spectrum of indicated nanocomposites. The vertical lines indicate the peak position. Inset shows the spectrum of pure nanoclay and PU.

Tuning of Structure and Morphology. The crystallinity varies in nanocomposites depending on nanostructure as evident from XRD and DSC studies. The intensity of the crystalline peak of pristine PU at ~23.9° increases for PI-NC while that is significantly reduced in PTMG-NC (Figure 3a). Distinct glass transition of pristine polymer becomes weaker in nanocomposites especially in exfoliated PTMG-NC (Figure 3b) due to constrained movement in the presence of rigid nanoclay. Depression of melting temperature in nanocomposites as compared to pure PU indicates stronger interaction between PU and organically modified nanoclay and PTMG-NC showing again nearly amorphous behavior (inset of Figure 3b). The endothermic peaks at ~25 °C are due to the melting of PTMG as confirmed from the melting pattern of pure polyol (PTMG). Pure PU exhibits flakelike morphology while that grain morphology gradually lesser in PI-NC and PP-NC followed by its disappearance in PTMG-NC (Figure 3c) strongly supports the XRD and DSC studies

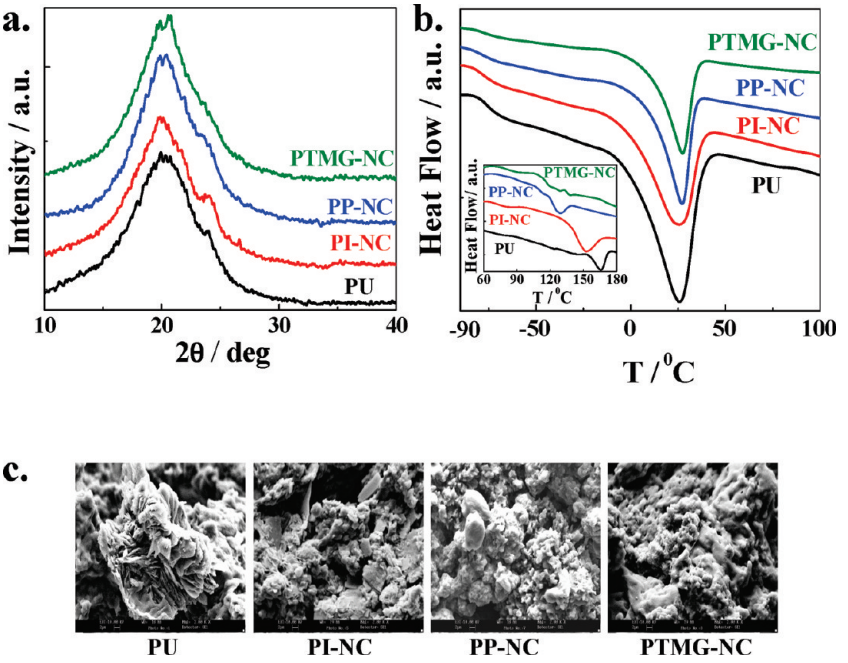

Figure 3. (a) XRD patterns of PU and its different nanocomposites. (b) DSC thermograms of PU and its nanocomposites in the second run. Inset shows the DSC first run for PU and its nanocomposites. The *Y*-axis has been shifted for the sake of clarity. (c) Scanning electron micrographs of PU and its indicated nanocomposites.

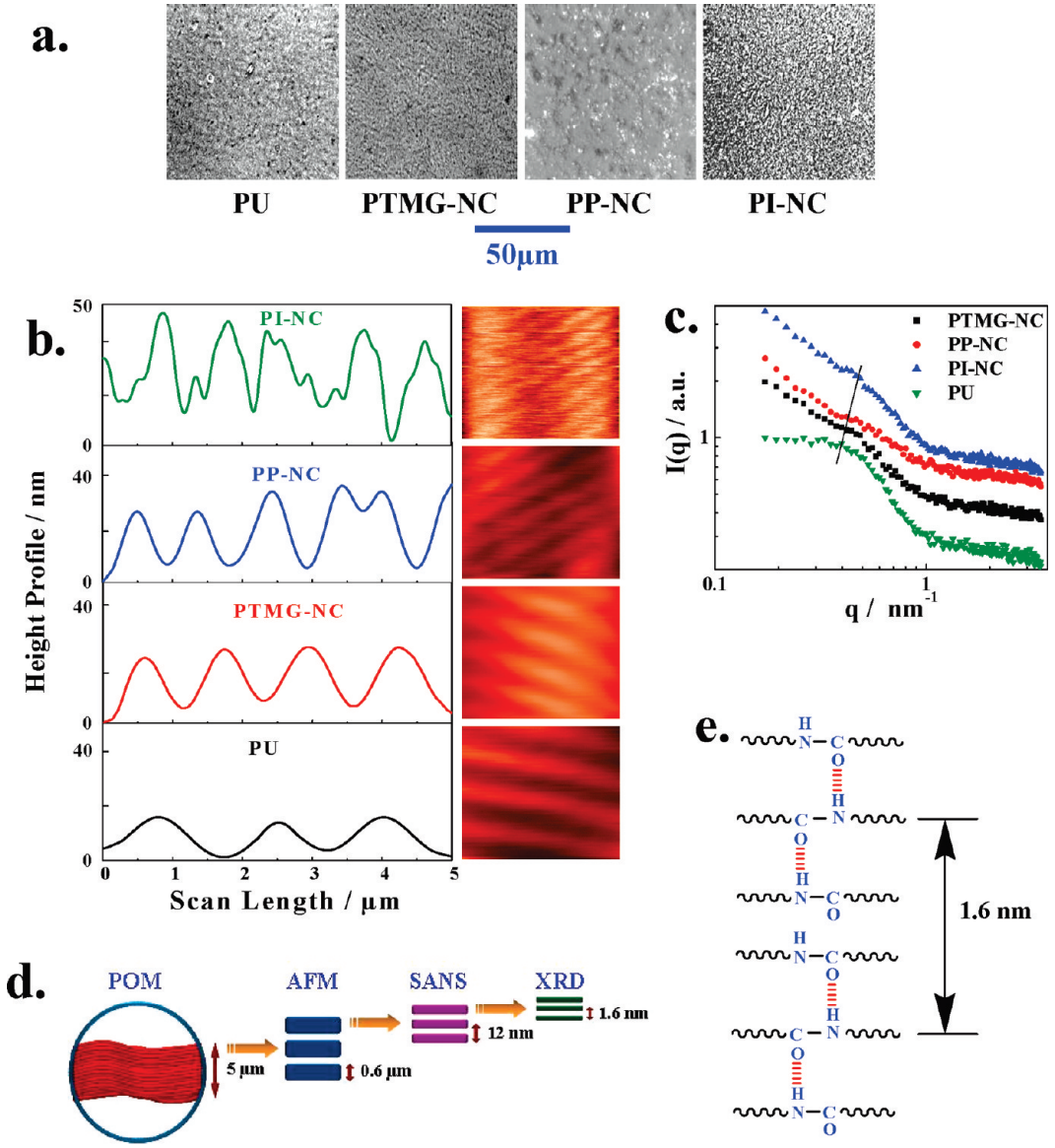

Figure 4. (a) Polarizing optical images of PU and its nanocomposites. (b) AFM images of PU and its nanocomposites (5 μm × 5 μm) obtained through tapping mode (right side figures). AFM height profile patterns for 5 μm scan length of PU and its nanocomposites shown in the left side of the figure. (c) Small-angle neutron scattering patterns; $I(q)$ vs q (wavevector) plot of indicated PU and nanocomposites. (d) Schematic representation of various dimension observable in different measuring devices. (e) Formation of molecular sheet through extensive hydrogen bonding (schematic approach) as measured using XRD.

that PI-NC and PP-NC are crystalline (ΔH = 6.8 and 4.5 J g^{-1}) but PTMG-NC is amorphous ($\Delta H \sim 0$) in nature. The similar effect has also been noticed in polyol crystallinity showing minimum for PTMG-NC (ΔH = 20 J g^{-1}) vis-à-vis 30, 28, and 25 J g^{-1} for pure PU, PI-NC, and PP-NC, respectively, further indicating the order of interaction in nanocomposites. Minute crystallinity in aliphatic PU helps improving the properties acting as a physical junction point against the aromatic polyurethanes which is predominantly amorphous. Moreover, tuning of crystallinity is another advantage using 2-D nanoparticles in different nanocomposites prepared through various routes.

Nanoparticle-Induced Self-Assembly. The domain structure in microscale is evident in pure PU which becomes prominent and organized for PI-NC and PP-NC while that is reduced in PTMG-NC (Figure 4a) under a cross-nicol optical microscope. More ordered cylindrical domains, within the above domain in optical micrographs, have been observed in AFM topographs in tapping mode for all the specimens (Figure 4b). Furthermore, the development of the small-angle neutron scattering (SANS) peaks at $q \sim 0.6$ nm^{-1}, corresponding to the characteristic length, Λ_c (= $2\pi/q_m$)~ 12−14 nm, indicates a nanostructure (Figure 4c) within the cylindrical domain as observed in AFM topographs. The lower value of Λ_c of nanocomposites (~12 nm) as compared to pristine PU (~14 nm) suggests the requirement of minimum number of molecular sheets to form an assembly in presence of 2-D nanoparticles. The bottom-up approach is obvious where nanostructure, exhibited by SANS peak, assembled to form a domain, observed in AFM, which further accumulated into microstructure/clusters noticeable in optical images, and the systematic assembly starting from nanostructure to microstructure is shown in Figure 4d. The nanostructure arising from polymer molecular sheet is further reflected in XRD (Figure 1b) peak at ~5.8° (d-spacing of 1.6 nm) in PI-NC is primarily due to greater interaction between polymer molecules through hydrogen bonding which is relatively less in the case of PP-NC and PTMG-NC as a result of

better dispersion and greater interaction between nanoclay and polymer chains originating from polymerization sequences. The said peak in XRD appears for PP-NC and PTMG-NC as well with higher hard segment PU where interchain hydrogen bonding is significant due to abundant urethane linkages (Supporting Information Figure S1), and the origin of the molecular stacking has been revealed through specific arrangement of hydrogen bonding leading to formation of molecular level sheet structure (Figure 4e). Two-dimensional molecular sheet is reported with numerous applications for π-conjugated polymers arising from π-stacking,[34,35] but this is so far the first ever instance of forming 2-D molecular sheet in thermoplastics even in amorphous phase. However, nearly 7−8 molecular sheets accumulate further to form a greater assembly emerged in the form of shoulder in SANS patterns ($\Lambda_c \sim 12-14$ nm). The SANS patterns are best fitted with the Ornstein−Zernike model (eq I) giving the correlation length, ξ, of all the samples in the range 3−3.6 nm showing the error bar (Supporting Information Figure S2).

$$I(q) = \frac{I(0)}{1+\xi^2 q^2} \quad \text{(I)}$$

where $I(q)$ is the scattered intensity and q is the wavevector.

The characteristic length ($\Lambda_c = 2\pi/q_m$, where q_m is the wavevector at peak maxima) gradually decreases as 14, 13, 12.5, and 12 nm for pure PU, PTMG-NC, PP-NC, and PI-NC, respectively, indicating close packing of lamellar distribution in nanocomposites, or in other words, a minimum number of molecular sheets are required for forming a lamellae in nanocomposites (9, 8, 7.5, and 7 for pure PU, PTMG-NC, PP-NC, and PI-NC, respectively, as calculated from individual Λ_c and 1.6 nm, the smallest possible distance between molecular sheet obtained from XRD peak), and few of those smaller assemblies further accumulate and become observable in AFM images. The greater assembly distribution, length, and height scale are very much reliant on various nanostructure/nanocomposites. The intensity of the height profile is significantly higher for nanocomposites as compared to pristine PU, indicating compact and dense crystallite in the presence of nanoclay. In addition, lesser numbers of assemblies are required to form an individual crystallite for nanocomposites, and the number of peaks in the height profile increases in the order of PU < PTMG-NC < PP-NC < PI-NC. Further zooming of a single crystallite shows a combination of a large number of smaller crystallite stipulates the step-by-step assembly of molecular sheet (Supporting Information Figure S3). The unique banded morphology in this material is due to extensive hydrogen bonding between molecular sheets as against the threadlike morphology observed in either aromatic or amine based PUs.[36−38] The crystalline domains in POM micrographs are the accumulation of many crystallites observed in AFM image. The average size of the crystalline domain increases for nanocomposites with respect to pristine PU. The driving force for this step by step self-assembly starting from nano- to micrometer scale is due to extensive hydrogen bonding between the polymer chains through urethane linkages. The stretching frequency of the >N−H bond of pure PU (3325 cm^{-1}) has shifted to lower frequency region for nanocomposites (~3313 cm^{-1}) which strongly supports the extensive hydrogen-bonded structure in nanocomposites together with their intense peak as compared to pristine PU (Supporting Information Figure S4).[39] Surprisingly, for polyurethanes containing aromatic diisocyanate or aromatic chain extender, the nanostructure and auxiliary self-assembly are missing presumably due to lack of hydrogen bonding in the presence of bulkier aromatic ring (Supporting Information Figure S5). Moderately strong secondary forces are supposed to be operating between molecules causing interlocking of the molecules/domains, leading to the formation of crystalline microdomain from nanoscale molecular sheet observed in XRD patterns to microscale crystalline domain observed in POM. However, the formation of nanostructure and subsequent self-assembly favors the creation of domain or microclusters in linear aliphatic polyurethane as well as its nanocomposites through XRD (1.6 nm), SANS (12−14 nm), AFM (0.6−1.5 μm), and POM (5−12 μm) in sequence, and the schematic bottom-up approach is shown in Figure 4d in general.

Modulation and Splintering of Network Structure. The mechanical responses under uniaxial stress have been shown in Figure 5a exhibiting higher stiffness for all the nanocomposites as compared to pristine PU. The elongation at break for PTMG-NC nanocomposites is even higher than that of pure PU. Toughness as measured from the area under stress−strain curves shows moderate increase for PP-NC and PI-NC while it dramatically improves (135%) for PTMG-NC (Figure 5b) due to exfoliated structure which helps suppress the crack propagation by orienting the individual silicate layers toward the applied force field.[40,41] In contrast, the modulus enhances a lot (~17 times) for PI-NC as a result of intercalation (sandwich effect) and flocculation of nanoclay which increase the ultimate aspect ratio of pure nanoclay cf. discussed in TEM morphology. Varying performance of composites, for a particular concentration of nanofiller, can be explained using Nielsen model[42] with adjustable parameters (A, B, and Ψ) to take into account the influence of microstructure on mechanical properties against the self-consistent model. Further, the strain recovery after fixed extension of 15% exhibit higher magnitude for PTMG-NC (73%) vis-à-vis pure PU (47%). PTMG-NC survives at least four cyclic loads each with 15% strain while pure PU and PI-NC and PP-NC break in third and fourth stretching, indicating the greater strength for PTMG-NC and builds the nanohybrid suitable for biological application (Supporting Information table). However, one can tune the stiffness, strength, and toughness of polyurethane by designing suitable nanocomposites using the same polymer and inorganic filler combination. The elongation at break is less as compared to elastomeric polyurethane as reported,[43] and the probable reason lies in the molecular weight. Our molecular weight was quite less as compared to the literature reported similar system where the molecular weight was 230 000. Similarly, the absence of strain-induced hardening is not observed because of lower molecular weight and low hard segment content of PU used in this study.

The networking due to the self-assembling of domains may have an impact on mechanical properties as compared to smaller domain dimension PU and its nanocomposites. The storage modulus, $G'(\omega)$, measured at $T_m + 20$ °C, increases for all the nanocomposites over a wide range of angular frequency ω (Figure 5c). Interestingly, the modulus exhibits a drop at specific range of ω depending on the type of nanocomposites followed by further enhancement with increasing frequency. The dip has been shifted systematically toward higher frequency in the order of PU < PTMG-NC < PP-NC < PI-NC, suggesting the breakage of networks primarily depends on the strength of association (superior for PI-NC because of intercalated and flocculated structure). One representative G' vs ω plot shows systematic lowering of dip frequency with increasing temperature, further strengthening the concept of correlating melt strength with the frequency of reorganization of network structure (Supporting

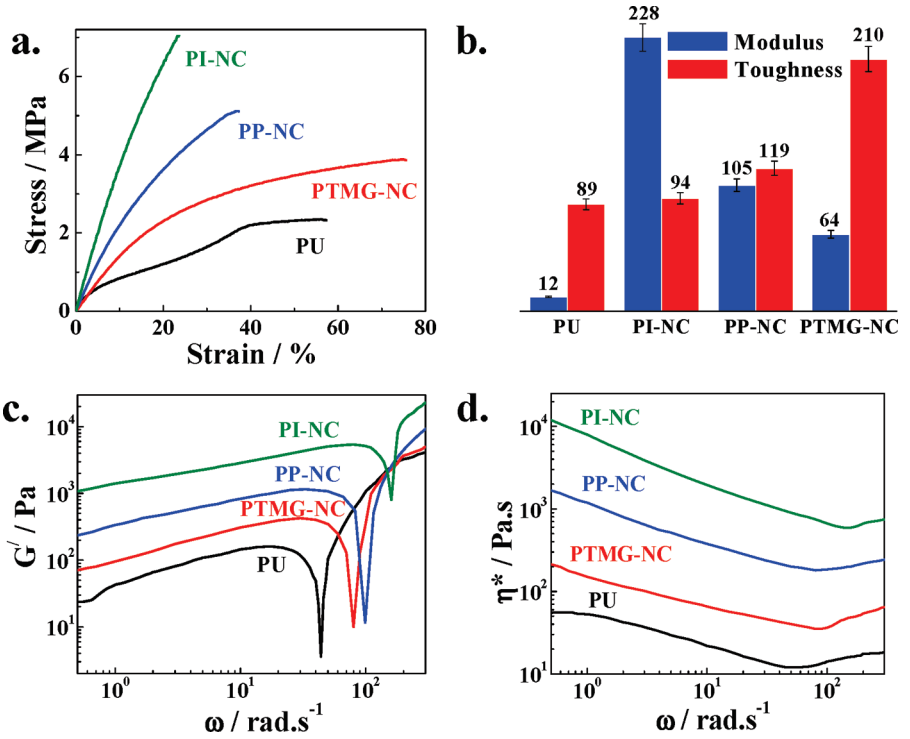

Figure 5. Mechanical behavior of PU and its nanocomposites: (a) stress−strain curves of pure PU and its nanocomposites; (b) comparison of modulus (MPa) and toughness (MJ m^{-3}) values of PU and its nanocomposites as indicated in the bar graph; (c) storage modulus; (d) complex viscosity of pure PU and its nanocomposites as a function of frequency at $T_{ref} = T_m + 20$ °C.

Information Figure S6). The fascinating phenomenon of splintering of structure occurs at higher frequency for nanocomposites as compared to pristine PU; the higher the strength of composite, the higher is the energy required to break the structure in the above-mentioned order. Subsequent enhancement of modulus after the plunge indicates the re-formation of structure, or in other words, the whole phenomena is considered as the reorientation/rearrangement of structure when the dynamic force of varying frequency applied to the materials. Similarly, the initial lowering of complex viscosities indicates the distortion of structure and attains a minima followed by enhancement due to restructuring (Figure 5d). The order of minima and the value of $\eta^*(\omega)$ follow the same trend as of storage modulus. Dynamic measurement also exhibits higher melt strength for nanocomposites as compared to pure PU, and among the nanocomposites, intercalated and flocculated composite (PI-NC) shows the highest strength (G' and η^*); the same trend is observed in stress−strain measurements. Hence, improved and tunable mechanical properties are achieved both in solid and in liquid phase for PU nanocomposites prepared using the same set of nanoclay (same content as well) and polymer constituents. The melt rheology also supports the formation of extensive networking in presence of nanoclay and the extent of which depends on the type of nanostructure. The origin of this networking lies in the formation of extensive intermolecular hydrogen bonding through urethane linkages which is again facilitated in the presence of nanoclay presumably due to extra hydroxyl group in the edges of 2-D nanoclay (intense FTIR ⟩N−H stretching peak). This unique splintering phenomenon appears to be due to discrete self-assembled crystallites bonded in amorphous matrix and is prone to rotational movement under stress field. The non-existence of networking or self-assembly pattern and subsequent insignificant mechanical property improvement in aromatic-based polyurethane are mainly due to the restriction of forming hydrogen bonds in proximity to the bulkier aromatic ring.[44] Aliphatic polyurethane has rather advantages and gets additional support from the organically modified nanoclay through self-assembly. Other improved properties of nanocomposites vis-à-vis pure PU are enhanced hydrophilicity (contact angles in advance mode are 65°, 60°, 59°, and 58° for pure PU, PI-NC, PP-NC, and PTMG-NC, respectively, showing better hydrophilcity in disperse system), gas barrier, and better UV absorption (Supporting Information) while maintaining its optical transparency pretty similar to pure polymer due to near amorphous character of polymer and nanometer size dispersed particles. Water absorption capability of nanocomposites (0.2 wt %) have significantly been reduced against 1.2 wt % for pure PU because of greater barrier property in the presence of a tortuous path created by 2-D nanoclays and makes the nanohybrid suitable for biomedical application even though the overall hydrophilic nature improves for nanocomposites as compared to pristine PU. In addition, the scratch hardness of the nanocomposite (300*g* force) has been improved 3-fold as compared to pristine PU (< 100*g* force) for a thickness of ~40 μm for every system.

Biological Recognition and Genotoxicity. Biocompatible commercial aromatic polyurethanes are being used in biomedical devices and implants.[45−50] Incorporation of nanoparticles into polymer matrix permits facile interaction to create a wide range of chemical and physical surface properties. For understanding the controlled cellular responses to implant polymeric materials/nano-biohybrid and to know about the regenerated tissue, cell adherence, and thereafter the cell particulars are important to study. These resorvable materials may induce a biological response and can construct certain architecture potentially harmful for long-term implant. Biological recognition must be carried out for the materials that reside in the body. With this aim in view, primarily HeLa and SiHa cells were allowed to grow on pure

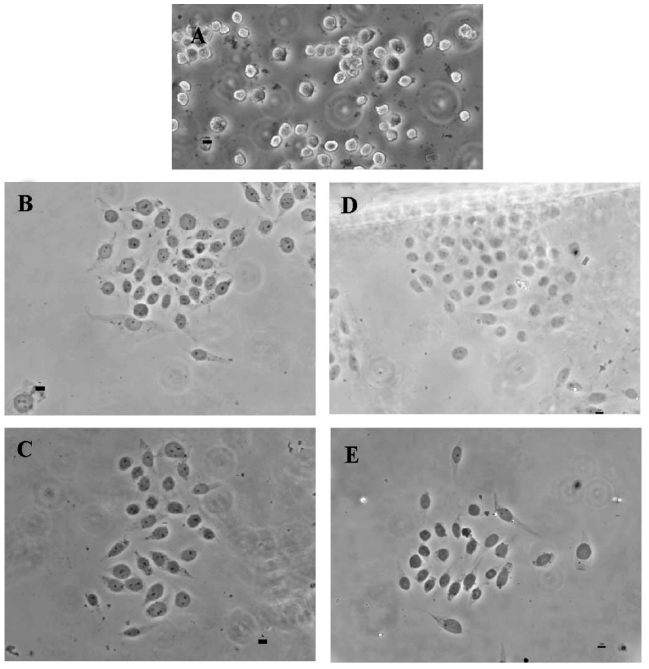

Figure 6. Phase-contrast images of cells grown on pure PU and its nanocomposites. Alteration of the shape of cells on PU after digested with trypsin at $t = 0$ (A). Cells in a healthy condition after adherence ($t = 48$ h) onto the surface of PU (B), PI-NC (C), PP-NC (D), and PTMG-NC (E) (scale bar = 10 μm).

PU and its nanocomposites. The cells used in this study are adherent type, which signifies that they are live, while the dead cells remain afloat on the media. After trypsin digestion, the cells were seeded onto the thin polymer film (pure and nanocomposites) coated onto a glass substrate. The cells got well-adapted to pure PU and its nanocomposite surfaces and adhered nicely to film surfaces. Phase-contrast images of the cultured cells (Figure 6) are healthy, providing a clear indication that the pristine PU and its various nanocomposites are compatible with the biological system. This was repeatedly observed (three times) even in 72 h culture. In order to have an in-depth perception of the effect of the polymer/nanocomposites on the health of the live cells in the context of genotoxicity, the subcellular localization of HIPK2 was checked. Cisplatin, a widely used chemotherapeutic agent, was used as a positive control for the production of genotoxic stress inside the cells, which in turn would trigger the hyperactivation of the kinase. When the cell experiences genotoxic stress, the endogeneous HIPK2 level gets elevated to circumvent such stressful condition and thereby initiates cascade, leading to apoptosis. HIPK2 is subsequently cleaved at arginine residues at 977 and 916 positions which removes the C-terminal autoinhibitory domain, leading to an increase in its ability to phosphorylate p53 at ser46.[27] The cleavage and the enhanced ability to phosphorylate p53 are known as the hyperactivation of HIPK2.[29] The subcellular localization of HIPK2 was determined by immunostaining with anti-HIPK2 antibody, followed by counting the number of cells having fluorescent signal in any of the three categories: (a) nuclear with little or no cytoplasmic signal, (b) cytoplasmic with little or no nuclear signal, and (c) both nuclear and cytoplasmic signals. We tried to corroborate the concentration of the drug (cisplatin), which can be used as a control in the experiment for revealing the biocompatibility status of nanocomposites for inducing genotoxic stress in cultured cells. The cells were treated with the different concentrations of the drug to

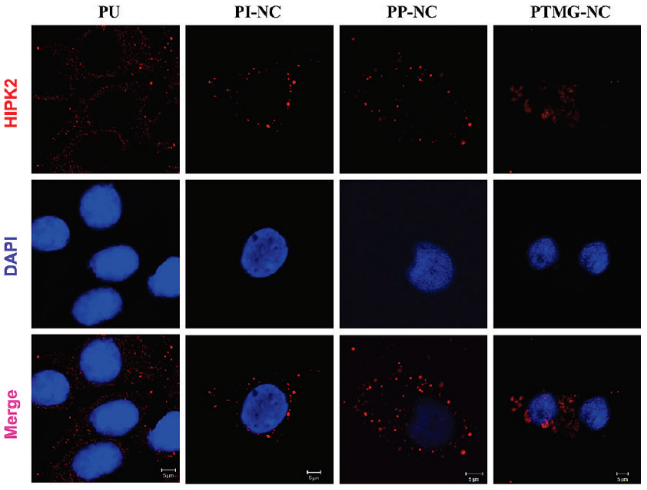

Figure 7. Confocal sections of HeLa cells grown on the surface of pure PU and its nanocomposites. The panel shows the localization of the pro-apoptotic activator, HIPK2, in the cells and appeared to be similar in all the categories. DAPI (4′,6-diamidino-2-phenylidone dihydrochloride) was used to counterstain the nucleus (scale bar = 5 μm).

observe the localization of the protein. Upon increasing the concentration to 7 μg mL^{-1}, cell death increased considerably, and hence, the initial experiment of fixing up the optimum concentration was restricted up to 6 μg mL^{-1}. There was a notable difference in HIPK2 subcellular localization observed in the concentration gradient of cisplatin. The percentage of cells having nuclear expression of HIPK2 increased with increase in the drug concentration (as evident in Supporting Information Figure S7). Antagonistically, the cytoplasmic localization decreased with increase in the nuclear localized fraction, barring in 6 μg mL^{-1}, where the nuclear fraction followed a decreasing trend. Hence, the optimized concentration of cisplatin treatment to sensitive cells for the induction of genotoxic stress and subsequently HIPK2 activation was kept at 5 μg mL^{-1} as a control, which coincides to the reported concentration. The staining pattern in the cells adhered to the different systems (PU, PI-NC, PP-NC, and PTMG-NC) was similar to the untreated one (0 μg mL^{-1}) (Figure 7 and control experiment in Supporting Information Figure S8). The HIPK2 speckles are found to be restricted to the cytoplasm only. The nucleus is almost devoid of any speckles and is incomparable to the control one (5 μg mL^{-1}). Our experiment as well as available literature provides a lucid impression of the cytoplasmic localization as a potent indicator of the inactive state of the protein and absence of any genotoxicity in the cell. In unstressed cells, a member of the high mobility group proteins, HMGA1, is overexpressed and causes the localization of HIPK2 to the cytoplasm. The alteration in the site of expression of HIPK2 alters its functional capability and renders it incapable in transactivating the pro-apoptotic genes, which is the molecular manifestation of the physiological status of the cell. Hence, the study elucidates that no genotoxic stress was induced on the cells using pure PU or its nanocomposites as surface for adhesion.

Conclusion

We demonstrated the advantages of adding two-dimensional nanoparticle in three different stages of polymerization, leading to widest possible range of nanostructure and to enhanced and unusual properties of nanohybrid materials. The relative microstructure arising from the varying interactions through absorption studies unravels the full potential of the nanocomposites

using the same polymer and organically modified inorganic filler. Layer by layer molecular assembly starting from nanoscale (1.6 nm) molecular 2-D sheet to microscale (~5 μm) crystallite through extensive secondary forces like hydrogen bonding in the presence of 2-D nanoparticles has been established for the first time for thermoplastics. Tuning of properties, especially the mechanical responses including the unique splintering phenomena, was made possible using a fixed concentration of nanoparticle by changing the route of synthesizing nanohybrids. For understanding the controlled cellular responses to the implant new hybrid materials, cell adhesion and detailed cytotoxicity and genotoxicity experiments have been carried out showing total biological recognition of the developed nano-biohybrids.

Acknowledgment. The authors acknowledge the research grant from Council for Scientific and Industrial Research (CSIR) Project No. 22(0399)/06/EMR-II. The authors also acknowledge the kind support of Dr. D. K. Avasthi, Mr. Pawan K. Kulriya, and Dr. Biswajit Ray of IUAC, New Delhi and Chemistry Department, BHU, for XRD, NMR, and GPC measurements. The authors gratefully acknowledge the kind support of Dr. S. Malik of IACS and Dr. M. Yashpal and Prof. G. Singh of IMS, BHU, for TEM measurements. The authors also acknowledge Dr. N. Misra of Biomedical Engineering, BHU, and Dr. A. S. K Sinha, Chemical Engineering, BHU, for contact angle and FTIR measurements, respectively. The authors acknowledge Mr. S. Nagarajan and Dr. B. S. R. Reddy, CLRI, for gas barrier measurements.

Supporting Information Available: Figures S1−S8 and table. This material is available free of charge via the Internet at http://pubs.acs.org.

References and Notes

(1) Bayer, O.; Muller, E.; Petersen, S.; Piepenbrink, H. F.; Windemuth, E. *Angew. Chem.* **1950**, *62*, 57–66.
(2) Oertel, G. *Polyurethane Handbook: Chemistry −Raw materials −Processing −Application −Properties*, 2nd ed.; Carl Hanser Verlag: Munich, 1993.
(3) Meckel, W.; Goyert, W.; Wieder, W. In *Thermoplastic Elastomers*; Legge, N. R., Holden, G., Schroeder, H. E., Eds.; Hanser Publishers: Munich, 1987.
(4) Liff, S. M.; Kumar, N.; McKinley, G. H. *Nature Mater.* **2007**, *6*, 76–83.
(5) Lendlein, A.; Langer, R. *Science* **2002**, *296*, 1673–1676.
(6) Versteegen, R. M.; Sijbesma, R. P.; Meijer, E. W. *Macromolecules* **2005**, *38*, 3176–3184.
(7) Wang, C. B.; Cooper, S. L. *Macromolecules* **1983**, *16*, 775–786.
(8) Koerner, H.; Price, G.; Pearce, N. A.; Alexander, M.; Vaia, R. A. *Nature Mater.* **2004**, *3*, 115–120.
(9) Maji, P. K.; Guchhait, P. K.; Bhowmick, A. K. *ACS Appl. Mater. Interfaces* **2009**, *1*, 289–300.
(10) Versteegen, R. M.; Kleppinger, R.; Sijbesma, R. P.; Meijer, E. W. *Macromolecules* **2006**, *39*, 772–783.
(11) Velankar, S.; Cooper, S. L. *Macromolecules* **1998**, *31*, 9181–9192.
(12) Zilg, C.; Thomann, R.; Mulhaupt, R.; Finter, J. *Adv. Mater.* **1999**, *11*, 49–52.
(13) Riess, G. *Prog. Polym. Sci.* **2003**, *28*, 1107–1170.
(14) Discher, B. M.; Won, Y. Y.; Ede, D. S.; Lee, J. C.; Bates, F. S.; Discher, D. E.; Hammer, D. A. *Science* **1999**, *284*, 1143–1146.
(15) Hadjichristidis, N.; Pispas, S.; Floudas, G. A. *Block Copolymer*; Wiley-Interscience: New York, 2003.
(16) Pochan, D. J.; Chen, Z.; Cui, H.; Hales, K.; Qi, K.; Wooley, K. L. *Science* **2004**, *306*, 94–97.
(17) Jain, S.; Bates, F. *Science* **2003**, *300*, 460–464.
(18) Christian, D. A.; Tian, A.; Ellenbroek, W. G.; Levental, I.; Rajagopal, K.; Janmey, P. A.; Liu, A.; Baumgart, T.; Discher, D. E. *Nature Mater.* **2009**, *8*, 843–849.
(19) Tomalia, D. A. *Prog. Polym. Sci.* **2005**, *30*, 294–324.
(20) Bosman, A. W.; Janssen, H. M.; Meijer, E. W. *Chem. Rev.* **1999**, *99*, 1655–1688.
(21) Gitsov, I.; Lin, C. *Curr. Org. Chem.* **2005**, *9*, 1025–1051.
(22) Gillies, E. R.; Jonsson, T. B.; Frechet, J. M. J. *J. Am. Chem. Soc.* **2004**, *126*, 11936–11943.
(23) del Barrio, J.; Oriol, L.; Sanchez, C.; Serrano, J. L.; Cicco, A. D.; Keller, P.; Li, M. H. *J. Am. Chem. Soc.* **2010**, *132*, 3762–3769.
(24) Osterbacka, R.; An, C. P.; Jiang, X. M.; Vardeny, Z. V. *Science* **2000**, *287*, 839–842.
(25) Sirringhaus, H.; Brown, P. J.; Friend, R. H.; Nielsen, M. M.; Bechgaard, K.; LangeveldVoss, B. M. W.; Spiering, A. J. H.; Janssen, R. A. J.; Meijer, E. W. *Nature* **1999**, *401*, 685–688.
(26) Andrade, J. D.; Hlady, V. *Adv. Polym. Sci.* **1986**, *79*, 1–63.
(27) Di Stefano, V.; Rinaldo, C.; Sacchi, A.; Soddu, S.; D'Orazi, G. *Exp. Cell Res.* **2004**, *293*, 311–320.
(28) Winter, M.; Sombroek, D.; Dauth, I.; Moehlenbrink, J.; Scheuermann, K.; Crone, J.; Hofmann, T. G. *Nat. Cell Biol.* **2008**, *10*, 812–824.
(29) Gresko, E.; Roscic, A.; Ritterhoff, S.; Vichalkovski, A.; Giannino del, S.; Schmitz, M. L. *EMBO J.* **2006**, *25*, 1883–1894.
(30) Puca, R.; Nardinocchi, L.; Pistritto, G.; D'Orazi, G. *Gynecol. Oncol.* **2008**, *109*, 403–410.
(31) Pierantoni, G. M.; Rinaldo, C.; Mottolese, M.; Benedetto, A. D.; Esposito, F.; Soddu, S.; Fusco, A. *J. Clin. Invest.* **2007**, *117*, 693–702.
(32) Wang, Z.; Pinnavaia, T. J. *Chem. Mater.* **1998**, *10*, 3769–3771.
(33) Xu, R.; Manias, E.; Snyder, A. J.; Runt, J. *Macromolecules* **2001**, *34*, 337–339.
(34) Chabinyc, M. L. *Polym. Rev.* **2008**, *48*, 463–492.
(35) Prosa, T. J.; Winokur, M. J.; Moulton, J.; Smith, P.; Heeger, A. J. *Macromolecules* **1992**, *25*, 4364–4372.
(36) Sheth, J. P.; Klinedinst, D. B.; Pechar, T. W.; Wilkes, G. L.; Yilgor, E.; Yilgor, I. *Macromolecules* **2005**, *38*, 10074–10079.
(37) Klinedinst, D. B.; Yilgor, E.; Yilgor, I.; Beyer, F. L.; Wilkes, G. L. *Polymer* **2005**, *46*, 10191–10201.
(38) McLean, R. S.; Sauer, B. B. *Macromolecules* **1997**, *30*, 8314–8317.
(39) Pattanayak, A.; Jana, S. C. *Polymer* **2005**, *46*, 3275–3288.
(40) Shah, D.; Maiti, P.; Gunn, E.; Schmidt, D. F.; Jiang, D. D.; Batt, C. A.; Giannelis, E. P. *Adv. Mater.* **2004**, *16*, 1173–1177.
(41) Shah, D.; Maiti, P.; Jiang, D. D.; Giannelis, E. P. *Adv. Mater.* **2005**, *17*, 525–528.
(42) Nielsen, L. E. *Mechanical Properties of Polymers and Composites*; Marcel Dekker: New York, 1974.
(43) Korley, L. T. J.; Liff, S. M.; Kumar, N.; McKinley, G. H.; Hammond, P. T. *Macromolecules* **2006**, *39*, 7030–7036.
(44) Mishra, A.; Aswal, V. K.; Maiti, P. *J. Phys. Chem. B* **2010**, *114*, 5292–5300.
(45) Hung, H. S.; Wu, C. C.; Chien, S.; Hsu, S. H. *Biomaterials* **2009**, *30*, 1502–1511.
(46) Baumgartner, J. N.; Yang, C. Z.; Cooper, S. L. *Biomaterials* **1997**, *18*, 831–837.
(47) Reddy, T. T.; Kano, A.; Maruyama, A.; Hadano, M.; Takahara, A. *Biomacromolecules* **2008**, *9*, 1313–1321.
(48) Wu, Z. Q.; Chen, H.; Huang, H.; Zhao, T.; Liu, X.; Li, D.; Yu, Q. *Macromol. Biosci.* **2009**, *9*, 1165–1168.
(49) Ding, M.; Li, J.; Fu, X.; Zhou, J.; Tan, H.; Gu, Q.; Fu, Q. *Biomacromolecules* **2009**, *10*, 2857–2865.
(50) Rinaldo, C.; Prodosmo, A.; Siepi, F.; Soddu, S. *Biochem. Cell Biol.* **2007**, *85*, 411–418.